IN-PLANE SHEAR BEHAVIOUR OF ADOBE MASONRY WALLETS STRENGTHENED WITH TEXTILE REINFORCED MORTAR

Paolino Cassese [1], Claudio Balestrieri [2], Luigi Fenu* [3], Domenico Asprone [2], Fulvio Parisi [2]

paolino.cassese@itc.cnr.it, claudio.balestrieri@unina.it, lfenu@unica.it, d.asprone@unina.it, fulvio.parisi@unina.it

[1]

Construction Technologies Institute (ITC)
Italian National Research Council (CNR)
Naples, Italy

[2]

Department of Structures for Engineering and Architecture
University of Naples Federico II
Naples, Italy

[3]

Department of Civil Engineering, Environment Engineering and Architecture
University of Cagliari
Cagliari, Italy

* corresponding author

ABSTRACT

Many people live in adobe masonry (AM) constructions in earthquake areas even if most of the existing constructions are not engineered, thus prone to seismic damage. Therefore, seismic retrofitting of existing AM structures is a critical issue. In this study, experimental results of diagonal compression tests on 21 adobe masonry wallets, before and after the installation of textile reinforced mortar (TRM) with either hemp or glass fibres, are presented. Hemp-TRM is found to be more effective than glass-TRM in improving the shear capacity of AM, showing a mean increase in shear strength and ductility of 25% and 260% in hemp-TRM-strengthened wallets and 12% and 100% in glass-TRM-strengthened wallets. The hemp textile allowed compatibility of the TRM to the masonry substrate, preventing premature debonding and local failure. Experimental results are compared to existing data on TRM systems made of vegetable fibres, evidencing a significant capacity enhancement through flax- and hemp-TRM systems.

Keywords: Adobe masonry; Hemp fibres; Experimental tests; Textile reinforced mortar; Shear behaviour; Ductility.

1 INTRODUCTION

Adobe masonry (AM) is one of the oldest and most widely used system for civil buildings and historical structures since 8000 B.C., even in seismic countries located in Latin America, Africa, India, Eastern Asia and Southern Europe [1-3]. Approximately, 15% to 17% of the world's population lives in earthen structures, which represent, in some regions, up to 40% of the existing buildings, especially in suburbs of high-density urban centres of developing countries [4,5]. Indeed, this solution is often pursued by underprivileged people who success in obtaining a low-cost dwelling, not seldom erected by residents themselves without any quality control [6]. Furthermore, such a structural typology is characterized by high seismic vulnerability that dramatically emerged over and over throughout recent history, frequently causing huge loss of life [7-10]. Principal reasons lie in the combination of heavy inertia masses and low mechanical strength, which is much lower in tension than in compression, which can produce sudden failure modes under earthquake loading. Nonetheless, it is noted that the quasi-brittle behaviour of the earthen material and its ductility depend on the specific mineralogical properties at the micro-scale, interaction/adhesion between elements at both meso- and macro-scales, and the type of fibre reinforcement [11].

Within this framework, during last four decades many researchers from all over the world were mainly involved in the complex challenge of (i) studying and, eventually, improving the construction materials, and (ii) identifying strengthening solutions able to combine cost efficiency and performance effectiveness by means of specific experimental activities. Main results from a literature review on these topics are dealt with in the following section, with the aim to highlight the research significance of the present study.

1.1 Literature review

The term 'adobe masonry' underlies traditional non-engineered production practice of bricks and mortar as well as construction techniques. Bricks are mostly made by mixing native soil and natural fibres according to local methods, whereas mud mortar with similar composition is used for joints. Numerous research studies are available in the literature on main aspects deeply affecting material mechanical response, such as soil mineralogical properties, water and fibre contents, stabilizers, production and curing steps [11–27]. Binici et al. [11] investigated the mechanical properties of mud bricks made with different combinations of fibrous waste materials and stabilisers. Those researchers concluded that, depending on the matrix-fibre interface, fibrous materials were able to improve the compressive strength of bricks. The effect of fibre length and fibre fraction on shrinkage, compressive strength, flexural strength, and shear strength was investigated in [12], considering four different soil classifications with chopped barley straw. Flexural strength increased as fibre fraction increases,

whereas enhancement of compressive strength was observed for a fibre fraction lower than 1.5% added to clayey silty soil and clay sandy soil. Achenza and Fenu [13] found that stabilization of earthen elements by means of natural polymers had a beneficial effect on their mechanical performance due to reduction of porosity. A notable influence of fibre length on the post-fracture response of earthen material with wool fibres under large deformations was found in [17], whereas a crucial dependence of mechanical response on the rate of loading was proved in [20] with reference to hemp-fibre addiction. A comprehensive study on the influence on uniaxial performance of adobe bricks depending on multiple variables, such as water and fibre content in the mixture, strain rate, soil constituents, and curing conditions, was addressed through experimental and numerical studies by Li Piani and his co-authors [24–27]. Those researchers found that high fibre contents can cause pauperization of mechanical response of adobe materials due to enhancement of porosity. Moreover, high sensitivity to loading rate depending on water content was revealed and modelled by means of proper rate-dependent numerical models.

The effectiveness of different retrofitting techniques has been addressed in literature mainly via experimental (seismic) shaking table testing on reduced-scale prototypes. Meli et al. [7] carried out an experimental study on the efficiency of different strengthening methods by means of seismic shaking tests on reduced-scale adobe houses. Those researchers identified in the welded mesh reinforcement the more viable solution, although a deeper investigation was needed. Technical procedures for seismic performance upgrading of monumental adobe structures were proposed in [2] based on the results of shaking table tests on both small-scale and large-scale prototypes reinforced with horizontal straps and bond beams. The effectiveness of plastic mesh reinforcement was assessed by Blondet et al. [28] through shaking table tests on a full-scale physical model of an adobe building. The unreinforced specimens suffered brittle failure, whereas the reinforced ones developed a satisfactory seismic response, allowing the authors to state that the best solution was represented by mesh placed on both sides of the walls installed with mud plaster. Alternative low-cost strengthening techniques based on rubber straps as post-tensioning system on the wall were investigated through shaking table tests on 1:10 scale masonry house in [29], proving to be a viable solution. Dowling and Samali [30] developed low-cost, low-tech reinforcement systems for adobe structures. Different solutions were applied to U-shaped adobe walls subjected to seismic loading. Test results indicated that a major improvement in structural performance was achieved using a grid system made of external/internal vertical and horizontal reinforcement (e.g., bamboo canes or wires connected to each other by ties placed in pre-drilled holes), and a timber ring/crown beam that restrained movement and enhanced the seismic resistance of the structure. Charleson [31] proposed seismic strengthening of earthen houses using straps cut from used car tires, delineating a

promising trade-off between very limited cost and seismic performance enhancement based on the results of shaking table tests. Shaking tests on a full-scale adobe housing prototype were performed in [32]. The damaged prototype was repaired by injecting cracks with a mud grout and tested again under the same dynamic motions. Test results indicated that the repairing technique was not adequate because only a reduced part of the original strength and stiffness were restored. Therefore, crack injection was found to require combination with strengthening systems. Torrealva [33] performed shaking table tests to investigate the efficiency of biaxial geogrids placed on both sides of adobe walls, connected to each other through wall thickness, and plastered with earthen mortar. That strengthening system drastically reduced the seismic vulnerability of earthen specimens. A similar study was presented in [34] wherein the effect of shaking orientation on response of specimens was also investigated, before and after strengthening with geogrids. Test results showed a considerable reduction of the seismic vulnerability of adobe wall structures. The efficiency of combined repair-strengthening techniques on a full-scale adobe dwelling was experimentally studied in [35] by means of shaking table tests under severe excitations. The as-built configuration was initially subjected to test. Then, the damaged model was subjected to both sealing of cracks via mud grout injection and strengthening by an external reinforcement made of a cheap nylon rope mesh externally bonded to the walls, and subsequently re-tested. That combined retrofit technique prevented excessive stiffness degradation and strength. Seismic behaviour of unreinforced and polypropylene (PP)-band retrofitted two-story masonry structures was evaluated through shaking table tests on reduced-scale specimens in [36]. The structure retrofitted with PP-band meshes showed a performance enhancement.

The above-mentioned experimental tests confirmed post-earthquake damage assessments highlighting that AM buildings frequently suffer local failure modes [37], including out-of-plane mechanisms of load-bearing walls and separation between orthogonal walls at building corners, due to poor seismic detailing (ineffective connections between orthogonal walls and lack of rigid floor systems). Less frequently, in-plane failure modes have been observed, generally related to a box-type global response of the building, which may effectively activate if local failure modes are prevented. In such a case, the improvement of shear strength and displacement ductility of AM walls against in-plane lateral actions becomes of paramount importance. Thus, both in-plane strength and ductility of walls significantly contributes to the seismic response of the whole structure, so the mitigation of seismic vulnerability should be based on prevention of local mechanisms and improvement of such capacity features. Nonetheless, fewer experimental studies focusing on the in-plane mechanical behaviour of unreinforced and strengthened real-scale AM walls and wallets under static loading have been found in literature. Cyclic test on real-scale adobe walls were carried out in [38], firstly in the

as-built configuration; then, injection of hydraulic lime grout and application of synthetic mesh incorporated in the plaster were executed. The solution proved to be very effective, restoring initial stiffness, increasing lateral strength and ductility, and avoiding brittle failure modes. Turanli and Saritas [39] presented an experimental investigation on the use of straw fibres, additives (i.e., fly ash) and plaster mesh by diagonal compression testing of adobe wallets. Specimens were divided into three groups with adobe blocks having different soil mixture, with and without mesh in mortar bed joints. Experimental results highlighted that the addition of either straw fibres or fly ash into adobe blocks enhanced the mechanical performance of wallets, whereas the use of cheap plaster reinforcement mesh in mortar bed joints increased both strength and energy absorption capacity. Figueredo et al. [40] carried out cyclic tests on real-scale walls that were repaired through lime gum injections into cracks and were strengthened via synthetic mesh fixed to the wall. Such a retrofit solution significantly improved the seismic performance of the adobe walls. Uniaxial compressive response of Chinese traditional adobe blocks and masonry prisms different for clay-silt contents was investigated in [19]. Masonry strength was not very sensitive to mortar strength and equal to about half of block strength. Diagonal compression tests on twelve identical unreinforced AM wallets were carried out in [41]. Sliding shear failure was observed with high dispersion of results in terms of both shear strength and strain. Static cyclic tests on an unreinforced half-scale adobe building were performed in [42] until significant cracking damage was observed. Then, cracks were injected by clay-based grout composed of the same soil of the AM materials and re-tested. Grouting proved to be a repair technique capable of partly restoring the initial stiffness and load-bearing capacity of the AM building, even if some technological issues were identified in the realization due to small width of cracks.

1.2 Research significance

In recent years, research studies on seismic vulnerability assessment of earthen buildings have increased also in Italy, where such constructions represent a non-negligible portion of the existing building stock in several regions [15, 43]. Among Italian regions, Sardinia island is currently characterized by the largest number of earthen dwellings, which represented the majority of the earthen constructions until the middle of the last century [44] and were usually made of adobe masonry. Sardinian adobe bricks were obtained by pressing a mixture of soil, water, and straw, into specific prismatic formworks and then exposed to natural drying (i.e., combined air-sunshine action). Stabilization of the adobe bricks' mixture was ensured by dung and urine in the past, whereas, more recently, cement and/or lime were added [1]. From a large-scale point of view, adobe structures in Sardinia were constructed based on traditional practice rules without any design. Only in the last decade, adobe buildings located in Sardinia have been

designed according to recent Italian code provisions [45–47] including simplified safety checks to earthquake actions.

The present study is part of a broad research programme focusing on assessment and mitigation of the seismic vulnerability of existing Sardinian adobe buildings [8, 44, 48–50]. The mitigation strategy is herein dealt with at structural component scale by means of an experimental campaign consisting in diagonal compression tests on AM wallets, before and after the installation of a strengthening system based on externally bonded textile reinforced mortar (TRM). Such investigation aimed at the evaluation of the strengthening efficiency of TRM on the in-plane response of AM walls, particularly in terms of strength and ductility, which represent key parameters for seismic performance of the whole building, provided that local mechanisms (e.g., due to scarce connections of consecutive walls) are prevented. Two different solutions for mortar reinforcement are considered as follows: (1) an innovative hemp-yarn grid, made of natural low-cost sustainable fibres and characterized by non-industrial production resulting in high variability of mechanical properties; (2) commercial glass-fibre meshes, which are usually adopted for masonry structures due to their good performance and moderate cost, as well as the availability of several design guidelines [51–53]. The viability of both hemp- and glass-textile reinforced mortar (here abbreviated as H-TRM and G-TRM, respectively) as strengthening system for adobe masonry structures is discussed in the following. After that the experimental programme is described, test results are presented and compared to those available in the literature, allowing some useful conclusions to be drawn.

2 EXPERIMENTAL PROGRAM

The experimental programme consisted of diagonal compression tests on both unreinforced and strengthened AM specimens. Major motivations behind this kind of tests to investigate the shear-compression behaviour included the minimal disturbance due to handling of specimens, limited cost and duration for set-up preparation, ability to provide valuable estimates of mechanical properties used in analytical models (e.g., [54]), and possible comparison with on-site tests performed on existing masonry constructions.

2.1 Materials

The constituent materials, namely adobe bricks and mud mortar, adopted for construction of AM wallets were already used in past studies wherein more detailed information about characterization procedures can be found [44, 48]. According to traditional Sardinian construction practice, adobe bricks were obtained by mixing native soil with water and straw fibres, following a completely non-industrial manufacturing process based on the Sardinian workers' expertise. Density and water content of the soil used for bricks were 2.68 g/cm^3 and 27%, respectively. The particle size distribution was characterized by the following percentages

by weight: 26.9% of clay and silt (grain diameter $d_g < 0.075$ mm), 70.1% of sand (0.075 mm $\leq d_g < 4.75$ mm) and 3% of gravel (4.75 mm $\leq d_g < 75$ mm), in tune with the typical ranges of that region. Accordingly, soil was classified as clayey-silty soil. Water and soil were firstly mixed, then, randomly oriented straw fibres with different dimensions were added. Subsequently, some water or soil was introduced, based on the mixture appearance evaluated by the manufacturer. Regarding straw fibres, a typical range of the fraction by weight in Sardinia is [0.5%, 3.0%], whereas the maximum fibre length is 100 mm. For the adopted adobe bricks, on average, straw fibres had diameter equal to 3 mm (with coefficient of variation CoV = 7%), 70 mm length (CoV = 34%) and 0.64% percentage by weight (CoV = 21%). The final shape was achieved by filling a prismatic wood formwork characterized by internal grooved surface. The mixture was pressed by hand until a certain degree of compaction was reached, also in this case without any measurement. The wet brick was left to dry to the sun. The resulting adobe bricks (see Figure 1a) had a mean unit weight of 16.80 kN/m^3 with CoV = 2%. Mud mortar, used for both masonry joints and TRM matrix, had the same soil composition of earthen bricks but without fibres, as typically made in Sardinian adobe masonry [8, 44, 48]. Nevertheless, a different amount of water was added during mixing operations until a 20% optimal water content by volume was reached, in tune with trend from the literature [19].

Uniaxial compression and three-point bending tests were carried out to assess mechanical properties of both adobe bricks and mud mortar. Specifically, compressive standard tests [55] were performed on 6 (for mortar) and 36 (for bricks) cubic specimens, from which mean values of compressive strength (f_c) equal to 0.50 MPa (CoV = 14%) and 1.08 MPa (CoV = 36%) were derived. Mean Young's modulus (E) associated with a stress level of $1/3f_c$ was found equal to 49 MPa (CoV = 40%) and 143 MPa (CoV = 47%) for mortar and bricks, respectively. The obtained performance in compression is partially not in tune with findings of several studies from the literature [24, 27, 50, 56]. As mentioned above, bricks and mortar are characterized by similar mixing, except for straw fibre inclusion that characterizes only the bricks. According to those studies, the presence of straw fibres in the mixture of adobe bricks reduces their strength and stiffness due to the significant increase in material heterogeneity, with weak interfaces in the soil matrix. As a result, compressive strength tends to decrease by increasing fibre content. Nevertheless, in some cases, fibres addiction can result into a compressive strength enhancement, essentially depending on soil composition [12]. This was the case of the material used in the present study, as confirmed in previous investigations on the same material [44], which is typical of Sardinia. A further possible reason for such result may lie in the fabrication process that includes a pressing phase of the soil-water-fibres mixture within the wooden formwork, acting in the direction of a potentially decreasing number of voids, hence improving interlayer bond. Standard three-point bending tests on specimens with size 40×40×160 mm^3, in

compliance with the European standard EN 1015-11 [57], were carried out for the evaluation of tensile properties. Specimens representative of brick material were sampled from the original units, whereas they were moulded into standard formwork for mortar characterization. A total of 8 tests were performed on mud mortar and 36 tests on adobe bricks. It is noted that a larger number of experimental tests were systematically conducted on bricks in order to properly take into account the further source of variability in mechanical response due to straw fibres with respect to mud mortar. On average, tensile strength (f_t) of adobe bricks was 0.56 MPa (CoV = 36%) whereas a lower value (f_t = 0.45 MPa with CoV = 20%) was obtained for mud mortar, as expected due to the absence of fibre reinforcement.

The glass fibre reinforced polymer (GFRP) grid was a biaxial alkali-resistant glass coated net with approximately 25 mm spacing, 225 g/m^2 unit weight, and 1.77% ultimate strain (Figure 1b). The grid was coated with a mixture based on a modified acrylic polymer. The mechanical properties, particularly Young's modulus and tensile strength, were provided by the supplier in terms of mean values E = 1276 MPa and f_t = 72000 MPa, respectively. It is noted that the supplier of the glass fibre grid did not provide dispersion measures of relevant properties.

The other reinforcing grid (Figure 1c) was a bidirectional 20×20 mm^2 mesh of hemp cords impregnated with a low-viscosity epoxy resin, according to the on-site procedure described in Section 2.2. The production process along with the experimental assessment of main mechanical properties for the single cord are described in detail in [58]. The single strand was obtained by twisting three hemp yarns, resulting in a final cord size of 3×400 tex. The dry hemp cords in their final twisted configuration were manufactured and supplied by Stabilimento Militare Produzione Cordami (Agenzia Industrie Difesa, Italy). The final resin content of each impregnated hemp cord was approximately 70% in volume. Given that the derivation of the actual stress for the hemp cord is not straightforward due to its diameter variability caused by resin impregnation, the tensile strength of the grid was experimentally obtained in terms of force per unit length of reinforcement, equal to 20 kN/m (CoV = 15%). Similarly, Young's modulus of the impregnated hemp cord was derived from data on the dry cord by assuming values of volumetric resin fraction that ranged between 6500 MPa and 7000 MPa.

Table 1 summarizes the main mechanical properties of all materials used in this study. Specifically, the mean value and CoV of compressive strength (f_c), tensile strength (f_t) and Young's modulus (E) are provided.

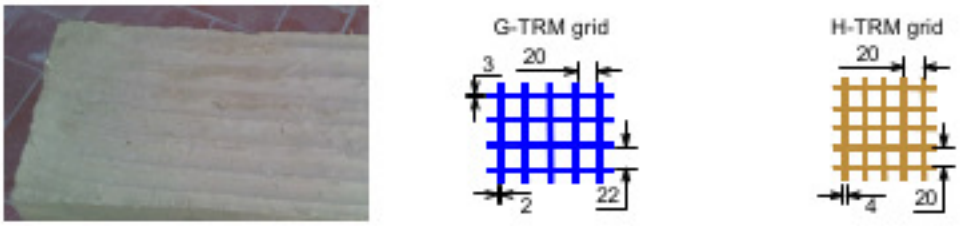

Figure 1 – Adobe brick and layout of reinforcing grids: (a) G-TRM and (b) H-TRM grid.

Table 1 – Mechanical properties of materials.*

Material	f_c (MPa)	f_t (MPa)	E (MPa)**
Adobe bricks	1.08	0.56	143
	[36%]	[36%]	[40%]
Mortar	0.50	0.45	49
	[14%]	[20%]	[47%]
Hemp grid	–	20 kN/m***	6500–7000
	–	[15%]	[*n.a.*]
Glass grid	–	1276	72000
		[*n.a.*]	[*n.a.*]

* *Values in square brackets are the coefficient of variation of the mechanical properties, if available.*

** *Young's modulus at one-third of the peak strength.*

*** *Tensile strength of the grid in terms of force per unit length of reinforcement.*

2.2 Description of specimens

Overall, twenty-one wallets were manufactured and tested. All specimens were made of straw fibre-reinforced adobe bricks (200×400×100 mm^3 in size) and mud mortar joints with thickness equal to 10 mm. Mortar had the same composition of adobe bricks but without fibres. The wallets consisted of two-leave adobe masonry with running bond configuration and total size of 410×1230×1230 mm^3 (Figure 2).

After fabrication, the specimens were equally divided into three different groups. The former was composed of unreinforced masonry wallets (URM series) and was tested without any strengthening system to simulate the as-built mechanical behaviour. The second group of specimens (HTRM series) was characterized by double-side strengthened wallets with H-TRM, whereas the third group of specimens (GTRM series) consisted of double-side G-TRM strengthened wallets.

The application of the TRM system (Figure 3) to each adobe wallet was carried out according to the following steps. After the external faces to be strengthened were moistened, a first mortar layer (with thickness equal to 10 mm) was applied and then the grid was placed and lightly pressed over fresh mortar. Finally, the face was finished by covering the grid with a 10-

mm-thick second layer of mortar. The total thickness of TRM system on each face was then equal to 25 mm.

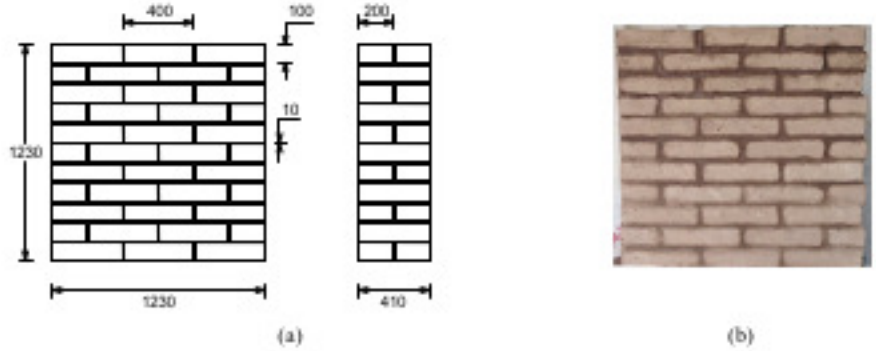

Figure 2 – Geometry and layout of unreinforced specimens: (a) frontal and transverse sections and (b) picture.

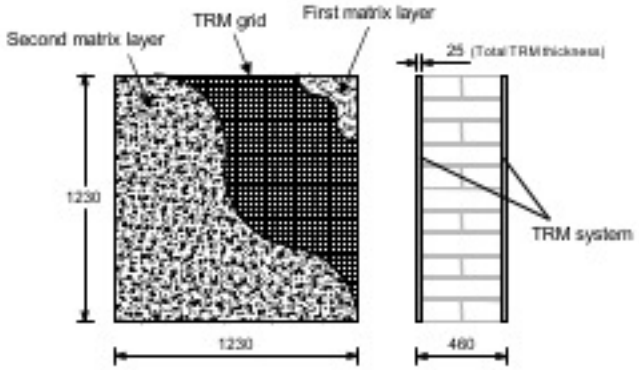

Figure 3 – Schematic representation of TRM strengthening systems.

Concerning the installation of the strengthening meshes, commercial glass-fibre grids were directly embedded in the mortar without any preparation; conversely, the hemp-fibre grids required a rigorous on-site fabrication. A 1300×1300 mm^2 wooden frame was firstly assembled. Then, nails were hammered on it with 20 mm spacing along both warp and weft directions, acting as support and guide for all the on-site hand-made grids. Thus, starting from the hemp yarn, the workers were able to manufacture the mesh by fixing and stretching the cord on the installed nails. Finally, a superficial coating with environmentally sustainable epoxy resin was applied, in order to prevent fibre degradation and to increase matrix-grid bond [59]. After curing, the grids were cut into square sheets of 1230×1230 mm^2 and installed. Accordingly, each wallet was strengthened on each side through a single mesh without any overlapping nor mechanical connection between TRM matrix (i.e., mud mortar) and grid. Main steps of the above-described procedure are summarized in Figure 4.

Figure 4 – Hand-made arrangement of H-TRM grid.

2.3 Test set-up, instrumentation and loading procedure

The masonry specimens were subjected to diagonal compression tests by means of the portable closed system schematically depicted in Figure 5a. The compression load applied along the diagonal plane of the wallet is the reaction force to the elongation of the hydraulic jack due to the double contrast. In order to prevent local stress concentration in specimen corners (resulting in possible premature crushing of the wallet), steel loading shoes were interposed between the hydraulic jack and the specimen on one side, as well as between the specimen and the contrast system on the opposite side (as suggested in [60]). The absence of a gap between specimen and steel shoe was guaranteed by filling with fast-setting, shrinkage-free mortar. The loading system was directly applied to the specimen into place of erection and, once installed, it was self-bearing (hence with no need for external supporting structures) and ready to use. To allow this, each specimen was erected on a rigid support block with proper height above ground. In line of principle, the support block provides balance to self-weight of the specimen, hence generating some state of normal (compressive) stresses within the specimen. However, it is expected that those stresses do not significantly influence the mechanical behaviour of the wallet in the region of interest (i.e., the central part of the specimen), also due to the lack of vertical contrast on top of the specimen. Furthermore, to avoid eventual panel-support friction affecting overall deformations, several layers of low-density foam material were interposed between the specimen and the support block. A picture of the installed system is shown in Figure 5b. The experimental set-up was selected because it strongly reduces disturbance of the specimen due to handling and transportation to laboratory, which a particularly relevant issue

for adobe masonry. Furthermore, the portable loading system was able to notably reduce efforts and time for testing execution and preparation, thus allowing both laboratory testing and on-site testing of existing masonry structures.

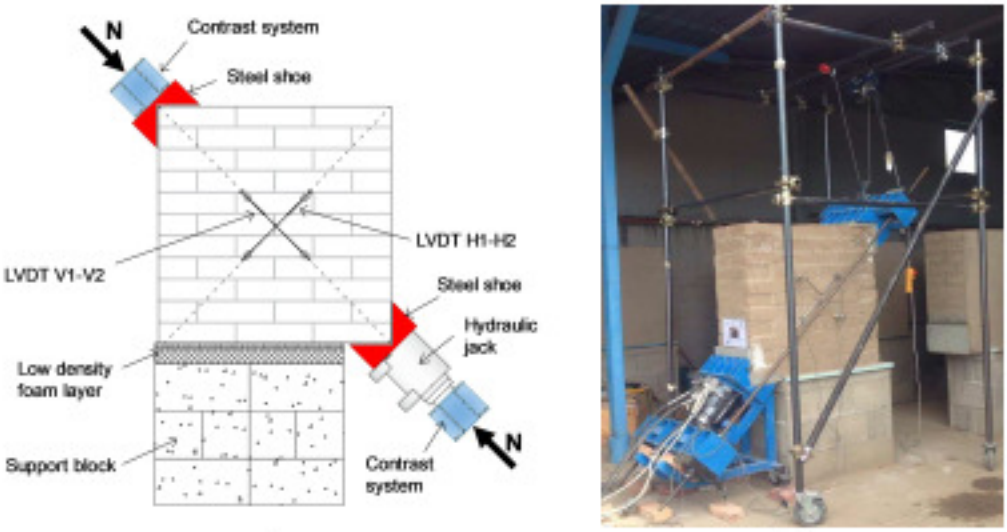

Figure 5 – Experimental set-up adopted for diagonal compression tests: (a) identification of components and (b) picture of specimen.

The tests were carried out by applying diagonal compression with displacement control at a rate of 0.01 mm/s until approximately 25% drop was observed with respect to the maximum recorded load on the post-peak softening branch of the force–displacement diagram. The testing machine was characterized by significant loading capacity (i.e., 500 kN) and total stroke of ±75 mm. In addition to the global control of the applied displacement and load, a proper instrumentation set-up was installed on each side of the wallet to measure the relative in-plane displacements along specimen diagonals (i.e., shortening and extension). Such a system was composed of four linear variable differential transformers (LVDTs) with gauge length g = 400 mm. More in detail, two LVDTs were installed on each side according to the scheme reported in Figure 5a. The displacements parallel to compression loading were tagged as ΔX_1 and ΔX_2 on sides #1 and #2, respectively, in line with the notation in ASTM E519-15 standard [60]. Similarly, perpendicular displacements were tagged as ΔY_1 and ΔY_2.

2.4 Data processing

The experimental response can be thoroughly understood through shear stress and shear strain (τ– γ) acting in the centre of the wallet properly derived from force and displacement values recorded by the instrumentation system. Specifically, force readings were processed according to RILEM TC 76-LUM guidelines [61] (abbreviated as RILEM hereinafter) and ASTM E519-

15 standard [60] (abbreviated as ASTM), which are based on different theoretical models for the interpretation of diagonal compression tests. The RILEM guidelines make use of the Frocht's solution for a homogeneous elastic isotropic shell [62], assuming a non-uniform flow of shear stresses along the loaded diagonal plane of the wallet. Conversely, the ASTM standard assumes a pure shear condition, resulting in a uniform distribution of shear stresses which (in absolute value) turn out to be principal tensile and compressive stresses. Based on these assumptions, shear stresses (τ_{RILEM}, τ_{ASTM}) in the centroid of the wallet were obtained through Eqs. (1) and (2), respectively, for the two test interpretation models [63], where: F is the value of the recorded diagonal compressive load corresponding to the imposed displacement; and A_n is the gross section area of the specimen. Such an area was computed according to the ASTM standard, as reported in Eq. (3), where: w, h, t are respectively the width, height, and total thickness of the specimen; and n is equal to 1 because the specimens had a solid cross section.

$$\tau_{RILEM} = 0.880 \cdot \frac{F}{A_n} \tag{1}$$

$$\tau_{ASTM} = 0.707 \cdot \frac{F}{A_n} \tag{2}$$

$$A_n = \left(\frac{w+h}{2}\right) \cdot t \cdot n \tag{3}$$

The average value of the displacements separately read by the LVDTs (i.e., parallel and orthogonal to the compressive load) installed on both specimen sides were divided by the gage length (g), in order to obtain axial strains ε_x and ε_y along shortening and extension directions, respectively (see Eqs. (4) and (5)). The nominal average shear strain (γ) of the specimen at each displacement step of the test was then computed as the sum of the afore-mentioned strains (as expressed by Eq. (6)).

$$\varepsilon_x = \frac{\Delta X_1 + \Delta X_2}{2g} \tag{4}$$

$$\varepsilon_y = \frac{\Delta Y_1 + \Delta Y_2}{2g} \tag{5}$$

$$\gamma = \varepsilon_x + \varepsilon_y \tag{6}$$

Finally, for each test, the τ–γ relationship between shear stress and shear strain was obtained for both RILEM and ASTM models from the experimental records processed

according to Eqs. (1) – (6). Based on each τ–γ diagram, the main capacity features of the wallet were defined as follows:

- τ_{max}: peak shear stress according to the selected guidelines (i.e., either RILEM or ASTM);
- τ_{cr}: cracking shear strain, assumed to be $\tau_{cr} = 0.7\tau_{max}$;
- γ_e: elastic shear strain, assumed to be associated with τ_{cr};
- G_e: elastic shear modulus, defined as $G_e = \tau_{cr} / \gamma_e$;
- G_i: initial shear modulus, defined as secant modulus associated with $0.25\tau_{max}$;
- γ_u: ultimate shear strain, corresponding to a 20% stress drop on the post-peak softening branch of the τ–γ diagram.

Accordingly, for each response curve (τ–γ), three performance levels (PLs) were identified as depicted in Figure 6, namely: cracking onset (PL1), corresponding to (γ_e, τ_{cr}); peak strength (PL2), corresponding to τ_{max}; and ultimate limit state (PL3), associated with γ_u.

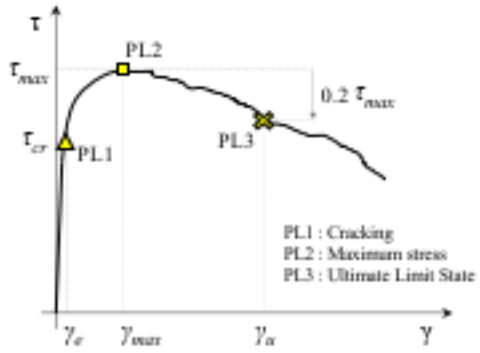

Figure 6 – Shear stress versus shear strain diagram and performance levels.

The ductility factor μ_γ accounting for energy dissipation capacity of the wallet was computed as the ratio of the ultimate shear strain to the elastic shear strain (i.e., $\mu_\gamma = \gamma_u / \gamma_e$). It is emphasised that the definition of the ductility factor is not univocal, as evidenced by various approaches currently available in the literature for the identification of both elastic (γ_e) and ultimate (γ_u) limit shear strains. The latter strain is usually associated with a shear stress drop equal to 15–20%, whereas a significantly higher variability in the definition of the limit elastic strain is observed. In some cases, γ_e was associated with the peak shear stress [58, 64], assuming that the specimen no longer behaves elastically after peak shear strength is reached. In other studies (e.g., [65]), γ_e is defined through a bilinear idealisation of the τ–γ diagram by assuming equal areas below the experimental and idealized response curves. As reported above, in the present study the elastic shear strain is assumed as corresponding to $\tau_{cr} = 0.7\tau_{max}$ and the ductility factor is assessed accordingly. Indeed, as described in the following section, the response curves were characterized by high dispersion among specimens in terms of shear strain during the post-cracking phase, particularly in relation to PL2, so a more robust assessment of experimental ductility capacity was obtained.

3 EXPERIMENTAL RESULTS

3.1 Experimental mechanical response

The results of the diagonal compression tests, processed according to both RILEM and ASTM models, are shown in Figure 7 in terms of shear stress versus shear strain (τ–γ) diagrams for all the specimens distinct in the three series URM, HTRM and GTRM. The mean value and CoV of the main capacity features of wallets, as defined above, are summarized in Table 2. The behaviour of the URM specimens was characterised by a pseudo-elastic branch, which was essentially linear up to the maximum shear stress, followed by a softening branch up to failure. Although a very similar elastic behaviour was observed on all specimens, the post-peak softening response was by contrast considerably scattered. More specifically, URM1 and URM5 specimens were characterized by a quite limited plastic branch with a ductility factor (μ_γ) equal to 9.2 and 11.8, respectively, as compared to the remaining specimens which showed a more important plastic capacity, characterized by μ_γ ranging between 15.7 and 20.5. In the case of URM7 specimen, a very high ductility was recorded ($\mu_\gamma = 28.9$). On average, the URM specimens were characterized by a ductility factor equal to 17.1, even if this result is affected by a relatively high dispersion (CoV = 41%). It is worth noticing that, as mentioned above, the shear strain (γ_{max}) corresponding to the peak shear stress (τ_{max}) was affected by very high dispersion (CoV = 114%), due to different damage evolution among specimens. The same was not recorded for strengthened specimens. For this reason, the ductility factor suggested for the URM series should be more properly characterized through the range [9.2, 28.9] rather than mean and CoV, hence resulting in a uniformly distributed random variable. Conversely, a small dispersion (CoV = 7%) in the peak shear stress (τ_{max}) was found, highlighting mean values equal to 0.133 MPa and 0.107 MPa according to RILEM and ASTM formulations, respectively. The same standards produced mean values of initial shear modulus (G_i) equal to 230 MPa and 185 MPa, with CoV = 33%. Finally, the mean elastic shear modulus (G_e) was equal to 125 MPa (RILEM) and 101 MPa (ASTM) with CoV = 13%. All H-TRM strengthened specimens exhibited a similar elastic-plastic response, with a pronounced post-cracking ascending branch (hardening behaviour due to TRM) up to the peak shear stress and a significant post-peak softening with quite limited slope (soft strength degradation). Data processing according to RILEM provided the following mean values: $\tau_{max} = 0.167$ MPa; $G_i = 265$ MPa; $G_e = 95$ MPa. Conversely, the ASTM formulation led to the following mean values: $\tau_{max} = 0.134$ MPa; $G_i = 213$ MPa; $G_e = 76$ MPa. The dispersion of such results was expressed by CoVs equal to 13%, 32% and 22%, respectively. As regards the ductility capacity, very high performance was obtained with mean value of the ductility factor equal to 61.4 and quite moderate dispersion (CoV = 22%), ranging between 41.2 (HTRM5 specimen) and 79.3 (HTRM4 specimen).

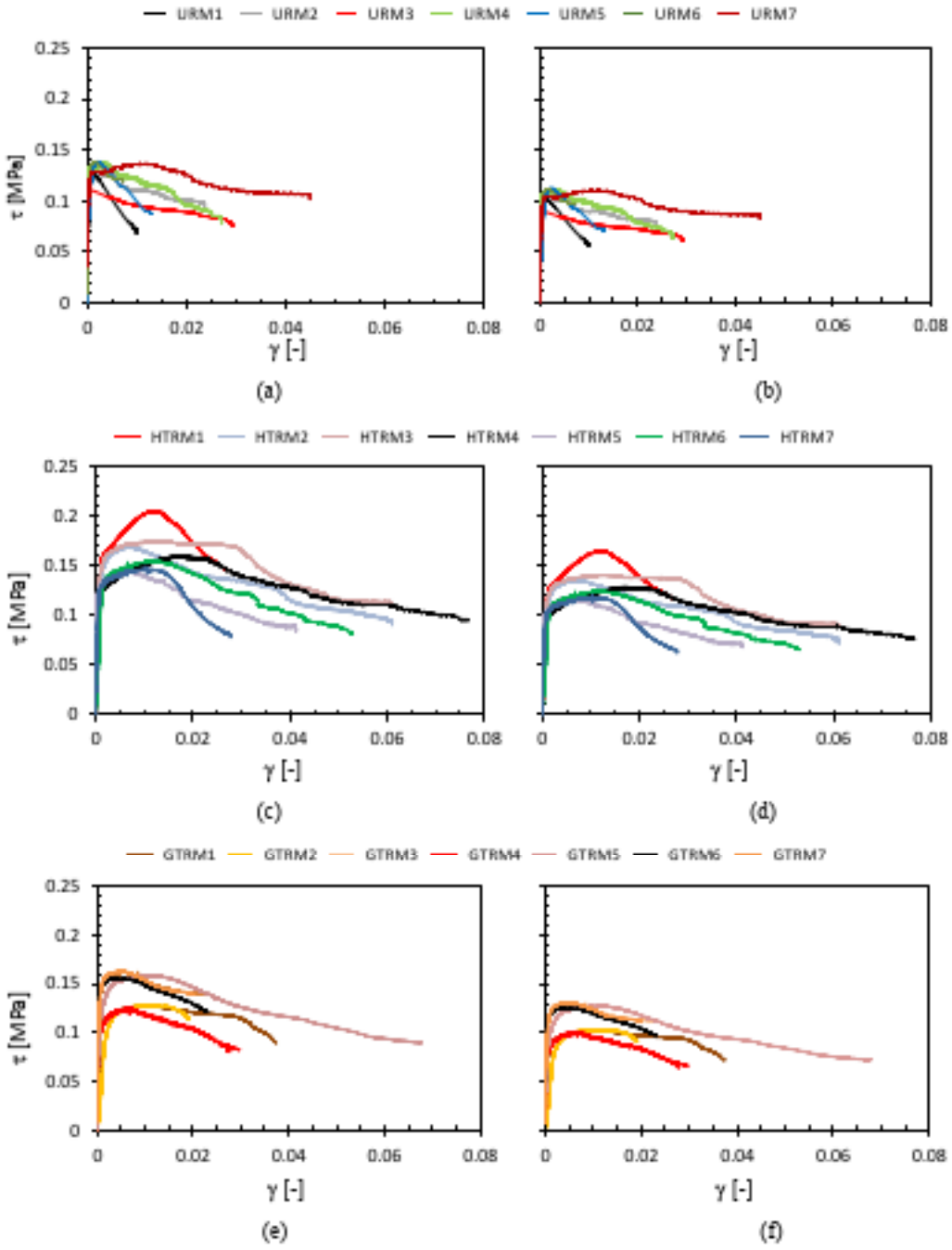

Figure 7 – Shear stress versus shear strain diagrams for URM, H-TRM and G-TRM specimens according to RILEM TC 76-LUM (a, c, e) and ASTM E519-07 (b, d, f).

A similar response was observed also on G-TRM strengthened specimens, characterized by a pseudo-elastic branch up to peak shear stress, with a slight post-cracking hardening, and a gradual post-peak softening up to failure. In this case, the RILEM formulation led to the following mean capacity features: $\tau_{max} = 0.149$ MPa; $G_i = 375$ MPa; $G_c = 169$ MPa, whereas data processing according to ASTM provided the following results: $\tau_{max} = 0.120$ MPa; $G_i = 300$

MPa; G_e = 136 MPa. A mean ductility factor of 38.2 and CoV = 19% were derived. Specifically, six of the seven specimens evidenced a ductility factor ranging between 32.2 (GTRM4 specimen) and 39.6 (GTRM5 specimen). Only in the case of GTRM1 specimen, a ductility factor of 51.6 was achieved.

Table 2 – Main capacity features of unreinforced and strengthened adobe wallets*.

Specimen type	γ_e (%)	γ_{max} (%)	γ_u (%)	μ_γ (-)	Standard	G_i (MPa)	G_e (MPa)	τ_{max} (MPa)
URM	0.08	0.33	1.37	17.1	RILEM	230	125	0.133
	[15%]	[114%]	[52%]	[41%]	ASTM	185	101	0.107
						[33%]	[13%]	[7%]
HTRM	0.13	1.33	7.57	61.4	RILEM	265	95	0.167
	[23%]	[35%]	[13%]	[22%]	ASTM	213	76	0.134
						[32%]	[22%]	[13%]
GTRM	0.06	0.77	2.38	38.2	RILEM	375	169	0.149
	[20%]	[42%]	[23%]	[19%]	ASTM	300	136	0.120
						[39%]	[19%]	[14%]

** Values in square brackets are the coefficient of variation (CoV) of the mechanical properties.*

As expected, test results in terms of shear strength (τ_{max}) and elastic modulus (G_i, G_e) derived via the two considered models (i.e., RILEM [61] and ASTM [60]) are systematically different. Since the adopted test set-up was expected to produce a negligible effect of compressive stresses within the central part of the specimen, further processing of experimental data, presented hereinafter, was carried out according to ASTM standard.

3.1.1 Discussion of results and trends

Response τ–γ curves were affected by significant dispersion within experimental groups, resulting in substantial differences in wallet mechanical performance. This was particularly evident in terms of ductility factor and for URM series. That variability can be related to several sources of uncertainties. Specifically, a key aspect statistically affecting masonry mechanical response is the combination of material properties variability with assemblage inhomogeneity [65]. Indeed, failure of masonry wallets subjected to diagonal compression test is generally governed by tensile strength of bricks located along transverse direction in the central part. Actually, the mechanical behaviour of masonry in diagonal compression may be regarded as a series system having the overall strength conditioned upon the strength of the weakest element (see Figure 8) considering both tensile strength and brick location as random variables. Further statistical variability is introduced by the presence of the TRM system, which is characterized by random variables such as mesh and matrix tensile strength, non-standardized fabrication procedure of meshes (especially for H-TRM), and geometrical inaccuracy deriving from the

installation process of TRM. With the aim to draw out some general trends regarding AM mechanical behaviour and TRM strengthening effects, the response variability must be take into account. Therefore, statistical analysis of the recorded stress–strain samples was carried out.

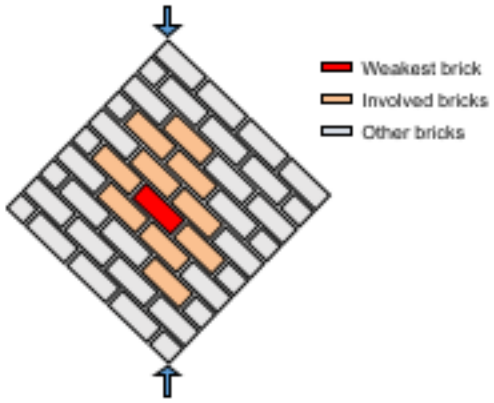

Figure 8 – Series system representative of URM wallet subjected to diagonal compression.

First of all, recorded shear stresses conditioned upon shear strains were assumed to be normally distributed random variables, allowing the computation of statistical stress–strain curves corresponding to 16th, 50th (median) and 84th percentiles of the above-mentioned conditional stress. Figure 9 shows a graphical comparison between such ordered statistics of the (τ–γ) experimental response for URM, H-TRM and G-TRM specimens, respectively. All curves were arrested to the ultimate shear strain (γ_u) corresponding to a 20% stress drop with respect to the peak shear strength, and the area surrounded by 16th and 84th curves of each series was evidenced. The scatter (S_τ) of the stress values was assessed as ratio of the difference between 84th and 16th values (τ^{84}, τ^{16}) to the median value (τ^{50}) given the shear strain (γ), as reported in Eq. (7) for the j-th series.

$$S_j(\gamma) = \frac{\tau_j^{84}(\gamma) - \tau_j^{16}(\gamma)}{\tau_j^{50}(\gamma)} \qquad j = URM,\ H\text{-}TRM,\ G\text{-}TRM \tag{7}$$

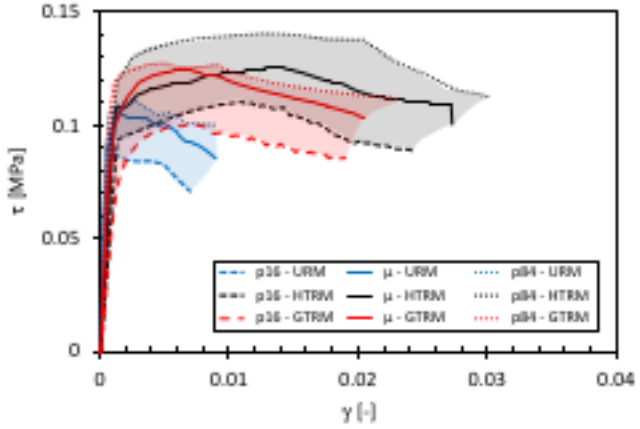

Figure 9 – Statistical τ–γ diagrams of URM, G-TRM and H-TRM specimens in terms of 16th, 50th and

84th percentiles of conditional shear stress, according to ASTM standard.

S_r distribution depending on the shear strain (γ) was almost uniform within the experimental group. On average, its value was equal to 26%, 39%, 25%, respectively for URM, H-TRM and G-TRM specimens; hence, the most dispersed results were recorded for the adobe masonry specimens strengthened with the H-TRM system. It is noted that similar findings were reported in [41]. By observing the percentile curves, some general trends may be identified concerning the overall mechanical behaviour shown by the different series. A significant post-peak shear strength degradation can be noted in the case of unreinforced specimens, the τ–γ response of which evolved along a steeper post-peak curve. Conversely, both H-TRM and G-TRM adobe wallets showed a post-peak softening that was considerably more gradual as well as a pronounced hardening phase prior to peak stress condition. Both TRM strengthening systems produced an increase in shear strength (τ_{max}) with respect to unreinforced condition; however, due to significant dispersion, a further statistical analysis was required to extrapolate a proper performance comparison. A similar issue affected also, and particularly, ductility factor (μ_γ), for which even wider ranges of variability were obtained within the experimental groups. Therefore, a different statistical approach was followed, based on the one-way analysis of variance (ANOVA) procedure, aimed at evaluating if the difference in terms of both strength and ductility between the three experimental groups (namely, URM, H-TRM and G-TRM) was statistically significant and then could be addressed to the variable *strengthening-system effect* or, conversely, the same was due to other uncertainty sources. To this aim, ductility factor (μ_γ) and strength (τ_{max}) values determined for the specimens of the three series were assumed as three mutually independent samples extracted from normally distributed populations. Then, according to ANOVA, the variance *between* and *within* the groups was computed and herein denoted as SS_b and SS_w, respectively. The so-called F-factor was thus calculated according to Eq. (8):

$$F = \frac{SS_b/df_b}{SS_w/df_w} \tag{8}$$

given the external and internal degrees of freedom (df_b and df_w, respectively) defined as $df_b = s - 1$ and $df_i = n - s$, with n equal to the total number of μ_γ (or τ_{max}) values and $s = 3$ (i.e., the number of samples). By assuming a significance level $p = 0.05$, F was compared to the test value F^* from Fisher's table. The main results of ANOVA for shear ductility and strength are summarized in Based on the results of ANOVA *F-test*, the so-called *null hypothesis* (corresponding to very similar mean values among samples) was rejected. Therefore, the difference in terms of $\mu\gamma$ and τmax between groups was statistically significant and, in other words, general trends on the mechanical behaviour exhibited by the three series can be derived from their respective mean values. Accordingly, the efficiency of each of the two analysed TRM systems in terms of shear strength gain with respect to the unreinforced condition was evaluated

via a synthetic factor ($\varepsilon\tau$) defined as ratio of the strengthened to unreinforced mean values of peak stress. Strength enhancement was significant especially in the case of H-TRM strengthened specimens, for which $\varepsilon\tau$ was equal to 1.25, whereas a lower gain was identified for the more conventional solution with G-TRM ($\varepsilon\tau$ = 1.12). Similarly, the efficiency of TRM systems in terms of ductility capacity was expressed through a synthetic parameter ($\varepsilon\mu$) obtained by dividing strengthened to un-strengthened ductility factor ($\mu\gamma$) mean values. H-TRM strengthened specimens exhibited a ductility capacity three times higher than URM ones, with $\varepsilon\mu$ equal to 3.6, whereas the more conventional solution with G-TRM system seems to provide less efficiency ($\varepsilon\mu$ = 2.2). Definitely, the capacity gain was particularly significant in terms of ductility which, as known, represents a key capacity feature for earthquake-resistant structures. Indeed, ductile strengthened walls contribute to the inelastic redistribution of seismic demand throughout the structure, so the higher is their ductility the larger are both displacement and energy dissipation capacities of the strengthened masonry structure. Conversely, a lower improvement is observed on shear strength, the increase of which can however be useful for seismic upgrading. H-TRM system provided higher performance than its G-TRM counterpart, probably due to the lower level of mechanical compatibility between high-performance glass mesh and mud mortar (i.e., TRM matrix).

Table 3 and Table 4, respectively.

Based on the results of ANOVA *F-test*, the so-called *null hypothesis* (corresponding to very similar mean values among samples) was rejected. Therefore, the difference in terms of μ_γ and τ_{max} between groups was statistically significant and, in other words, general trends on the mechanical behaviour exhibited by the three series can be derived from their respective mean values. Accordingly, the efficiency of each of the two analysed TRM systems in terms of shear strength gain with respect to the unreinforced condition was evaluated via a synthetic factor (ε_τ) defined as ratio of the strengthened to unreinforced mean values of peak stress. Strength enhancement was significant especially in the case of H-TRM strengthened specimens, for which ε_τ was equal to 1.25, whereas a lower gain was identified for the more conventional solution with G-TRM (ε_τ = 1.12). Similarly, the efficiency of TRM systems in terms of ductility capacity was expressed through a synthetic parameter (ε_μ) obtained by dividing strengthened to un-strengthened ductility factor (μ_γ) mean values. H-TRM strengthened specimens exhibited a ductility capacity three times higher than URM ones, with ε_μ equal to 3.6, whereas the more conventional solution with G-TRM system seems to provide less efficiency (ε_μ = 2.2). Definitely, the capacity gain was particularly significant in terms of ductility which, as known, represents a key capacity feature for earthquake-resistant structures. Indeed, ductile strengthened walls contribute to the inelastic redistribution of seismic demand throughout the structure, so the higher is their ductility the larger are both displacement and energy dissipation

capacities of the strengthened masonry structure. Conversely, a lower improvement is observed on shear strength, the increase of which can however be useful for seismic upgrading. H-TRM system provided higher performance than its G-TRM counterpart, probably due to the lower level of mechanical compatibility between high-performance glass mesh and mud mortar (i.e., TRM matrix).

Table 3 – Main results of the one-way ANOVA test in terms of ductility factor (μ_δ).

Source	*SS*	*df*	*p*	*F*	F^*	*F-test*
Between (*b*)	5883.4	2	0.05	37.0234	3.6823	$F > F^*$
Within (*w*)	1430.2	18				
Total	7313.6	20				

Table 4 – Main results of the one-way ANOVA test in terms of shear strength (τ_{wall}).

Source	*SS*	*df*	*p*	*F*	F^*	*F-test*
Between (*b*)	0.0023	2	0.05	6.7797	3.6823	$F > F^*$
Within (*w*)	0.0030	18				
Total	0.0053	20				

The experimental shear stiffness degradation with the shear strain was finally addressed in this study. Specifically, the relationship between the normalized secant shear modulus (G/G_i) of the adobe masonry wallets and normalized shear strain (γ/γ_i), the latter assumed to be corresponding to a shear stress value equal to $0.5\tau_{max}$, is reported in Figure 10, for all test series. It is noted that the graph is stopped to a shear strain ratio $\gamma/\gamma_i = 31$, for the sake of clarity. As expected, a very steep degradation of the secant shear modulus is observed with the displacement demand on the wallet, which is consistent with the rapid development of damage (early cracking) due to poor mechanical behaviour of both bricks and mortar. The same trend is observed also for strengthened wallets, which however reached higher values of γ/γ_i. As known, the strengthening effect of the reinforcing mesh increases up to the attainment of peak strength, when the damage state is anymore extensive and irreversible. In nonlinear numerical analysis of AM structures under seismic loads based on either distributed plasticity macro-element models [66] or finite element macro-models [67–70], a relationship expressing the shear stiffness under increasing shear strain can be particularly useful to account for shear strength degradation due to the displacement demand on a given wall beyond cracking onset. Therefore, a statistical fitting of the experimental $G/G_i - \gamma/\gamma_i$ curves was carried out herein. A negative-power decreasing trend described by Eq. (7) provides the best-fitting results for the post-cracking phase, with a coefficient of determination $R^2 = 0.987$.

$$\frac{G}{G_i} = 1.14\left(\frac{\gamma}{\gamma_i}\right)^{-0.575} - 0.1096 \quad \text{if } \frac{\gamma}{\gamma_i} \geq 1 \tag{7}$$

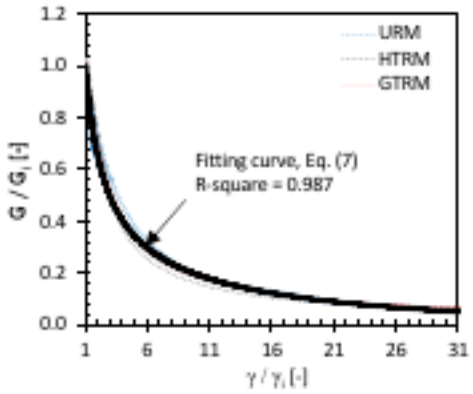

Figure 10 – Secant shear modulus versus shear strain normalized to their elastic estimates.

3.2 Description of the observed damage

Most of unreinforced specimens were characterized by the development of similar cracking patterns and failure modes (see Figure 11) with wide passing-through diagonal cracks. Due to the similar composition of mud mortar and adobe bricks, cracks were partially stair-stepping and involved both joints and bricks. As expected, diagonal tension failure mode occurred due to stress concentration along the tensile principal direction. Such shear failure mechanisms led to a rather poor post-peak softening response with limited ductile behaviour, except for URM7 specimen that suffered cracks mostly in adobe bricks. The damage observed on the wallets strengthened with the two different TRM systems was considerably different. Cracking pattern developed on H-TRM wallets was almost uniform over the entire specimen series. Diagonal cracks appeared on both wallet sides along the compressed diagonal, which globally followed the stair-stepped direction of the inner unreinforced adobe masonry (Figure 11a). As the crack width increased, the hemp grid gradually reached its ultimate strain up to fracture (Figure 11b). No premature debonding between the hemp grid and mortar, neither local failure of the grid, was observed. Tensile stress of the inner masonry was transferred through the matrix to the hemp chords progressively up to their failure. That behaviour was enabled by the properties of hemp grid, the limited stiffness of which was comparable to the mortar stiffness. The H-TRM strengthening system proved to be particularly effective due to its compatibility with both matrix and masonry, leading to considerable increase in strength and, particularly, ductility capacity of the wallet.

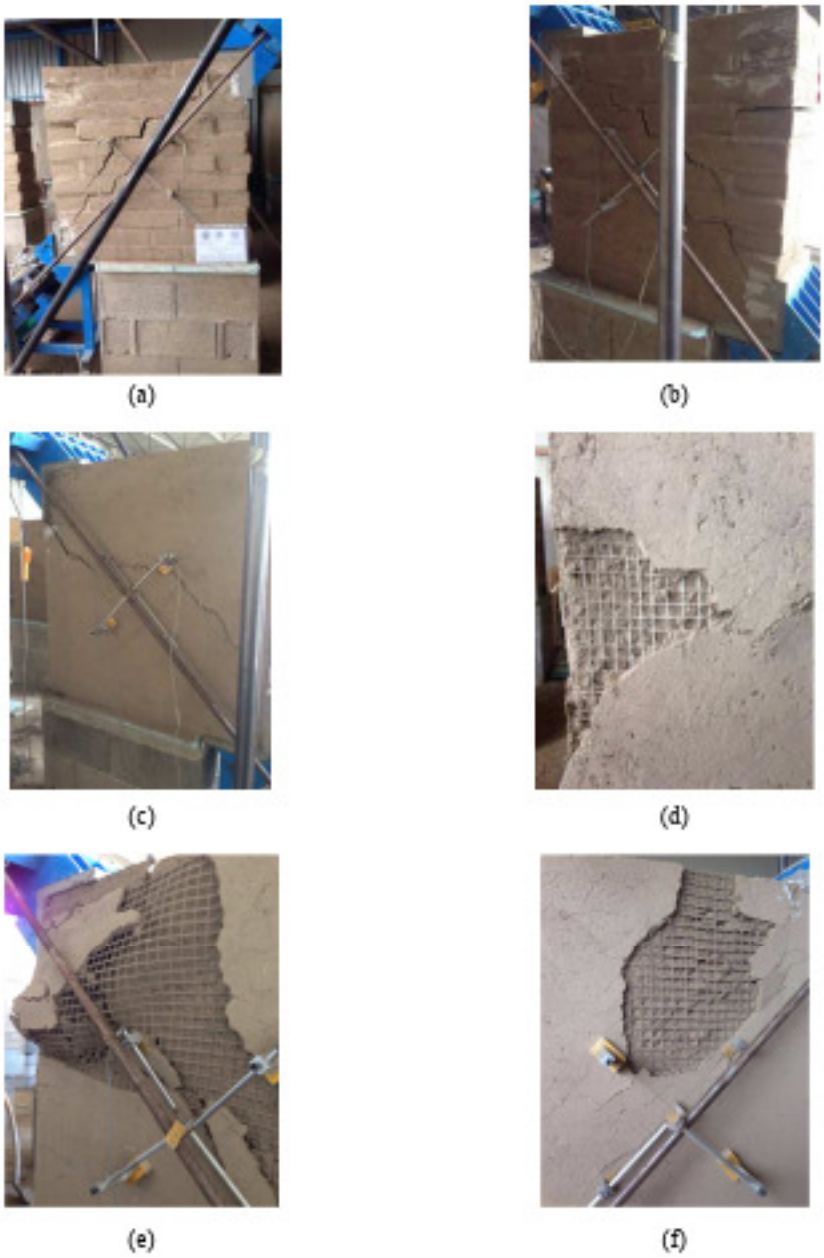

Figure 11 – Typical crack patterns: unreinforced masonry specimens at failure on sides A (a) and B (b); H-TRM strengthened specimens at failure (c) and detail of the grid rupture (d); G-TRM strengthened specimens at failure with local debonding details on sides A (e) and B (f).

Conversely, the damage evolution observed on G-TRM strengthened specimens highlighted a local detaching of the strengthening system, with delamination and debonding phenomena during the post-peak phase. Initial cracks developed along the loaded diagonal and increased their width until locally the glass grid was not able to follow the matrix deformation, then resulting in a local failure of the G-TRM system (Figure 11). Such a phenomenon was mainly due to the insufficient mechanical compatibility between glass mesh and mud mortar. Finally, no out-of-plane deformations were visually identified on the strengthened specimens after the

tests. It is also emphasised that no local failure of masonry close to the steel shoes was observed, even though a significant stress concentration was induced at those locations by compressive loading.

4 COMPARATIVE ANALYSIS

In order to deeply investigate the strengthening performance of H-TRM for adobe masonry walls, a comparative analysis was carried out in this study. To this aim, experimental studies on the assessment of the in-plane shear behaviour of masonry wallets strengthened with vegetable-fabric TRM were reviewed. Due to the high novelty and unconventionality of such a strengthening technique, only three research works were found in the literature [58, 64, 71]. Menna et al. [58] investigated the influence of H-TRM systems on the in-plane shear behaviour of masonry wallets, made of both Neapolitan yellow tuff (NYT) and clay bricks. Two different mortar types were considered for the matrix, i.e., pozzolanic and natural hydraulic lime (NHL), for a total of 12 masonry wallets subjected to diagonal compression tests. An anchor system consisting in five T- or L- shaped hemp ties was installed on each side of the specimens in order to avoid possible local failure. Ferrara et al. [64] presented the results of an experimental study on the shear capacity of wallets strengthened by two TRMs characterised by different amounts of flax mesh. Three series of three masonry specimens with clay brick and NHL mortar were tested under diagonal compression in unreinforced, single-layer and double-layer strengthened configurations, respectively. In this latter case, the outer layer was completely overlapped to the inner layer, after the application of an intermediate mortar layer. Relevant properties of specimens were collected in a proper experimental database and testing results were analysed. Mercedes et al. [71] performed sliding shear cyclic tests on 10 masonry wallets made of clay bricks and NHL mortar. Cementitious matrix was used for the TRM system and three different mesh typologies made of glass, cotton and hemp fibres were investigated. Each specimen was strengthened on each side through a single mesh without any overlapping nor mechanical connection.

Experimental data collected from the selected studies are outlined in Table 5. In line of principle, a direct comparison between the collected test results and those presented in this study is possible for few tests of Table 5. In fact, hemp reinforcing meshes were applied only by Menna et al. [58] on all specimens and by Mercedes et al. [71] on two specimens. Nevertheless, in the latter study, experimental results were obtained from cyclic shear tests according to a test procedure derived from ASTM E2126 standard [72], so the comparison is not straightforward. Conversely, Ferrara et al. [64] considered only flax grid as TRM reinforcement. Therefore, with reference to the experimental results reported in [58], a comparison of performance exhibited by the H-TRM strengthening system when applied to different masonry typologies is carried out herein. Main outcomes are summarized in Table 6.

Table 5 – Main properties of specimens considered in the database.

Source	Spec. ID	Masonry type*		TRM type		Wallet size (mm)		
		Bricks	Mortar	Textile	Matrix	$L \times H \times t$		
Menna et al. [58]	NYT-P1	NYT	P + NHL	-	-	1200	1200	250
	NYT-P2	NYT	P + NHL	-	-	1200	1200	250
	NYT-HFC_PT_1	NYT	P + NHL	Hemp	P	1200	1200	280
	NYT-HFC_PT_2	NYT	P + NHL	Hemp	P	1200	1200	280
	NYT-HFC_MW_1	NYT	P + NHL	Hemp	NHL	1200	1200	320
	NYT-HFC_MW_2	NYT	P + NHL	Hemp	NHL	1200	1200	320
	C-P1	Clay	P + NHL	–	–	1200	1200	250
	C-P2	Clay	P + NHL	-	–	1200	1200	250
	C-HFC_PT_1	Clay	P + NHL	Hemp	P	1200	1200	280
	C-HFC_PT_2	Clay	P + NHL	Hemp	P	1200	1200	280
	C-HFC_MW_1	Clay	P + NHL	Hemp	NHL	1200	1200	320
	C-HFC_MW_2	Clay	P + NHL	Hemp	NHL	1200	1200	320
Mercedes et al. [71]	WN1	Clay	NHL	-	-	1000	900	128
	WN2	Clay	NHL	-	-	1000	900	128
	WMN1	Clay	NHL	-	NHL	1000	900	148
	WMN2	Clay	NHL	-	NHL	1000	900	148
	WH1	Clay	NHL	Hemp	NHL	1000	900	148
	WH2	Clay	NHL	Hemp	NHL	1000	900	148
	WC1	Clay	NHL	Cotton	NHL	1000	900	148
	WC2	Clay	NHL	Cotton	NHL	1000	900	148
	WG1	Clay	NHL	Glass	NHL	1000	900	148
	WG2	Clay	NHL	Glass	NHL	1000	900	148
Ferrara et al. [64]	USW-1	Clay	NHL	-	-	1030	1030	120
	USW-2	Clay	NHL	-	-	1030	1030	120
	USW-3	Clay	NHL	-	-	1030	1030	120
	SW-1L-1	Clay	NHL	Flax	NHL	1030	1030	130
	SW-1L-2	Clay	NHL	Flax	NHL	1030	1030	130
	SW-1L-3	Clay	NHL	Flax	NHL	1030	1030	130
	SW-2L-1	Clay	NHL	Flax	NHL	1030	1030	136
	SW-2L-2	Clay	NHL	Flax	NHL	1030	1030	136
	SW-2L-3	Clay	NHL	Flax	NHL	1030	1030	136

** NYT : Neapolitan Yellow Tuff; NHL : Natural Hydraulic Lime; P : Pozzolanic*

Table 6 – Comparison of mean performance of H-TRM system on different masonry typologies*.

Masonry type	Unreinforced specimens		H-TRM strengthened specimens		Performance ratios	
	$\tau_{max,u}$ (MPa)	$\mu_{\gamma,u}$ (-)	$\tau_{max,s}$ (MPa)	$\mu_{\gamma,s}$ (-)	$\tau_{max,s}/\tau_{max,u}$ (-)	$\mu_{\gamma,s}/\mu_{\gamma,s}$ (-)
NYT	0.33	1.0	0.78	4.6	2.3	4.6
Clay	0.18	1.0	0.94	19.8	5.4	19.8
Adobe	0.13	17.0	0.17	61.0	1.3	3.6

** Shear stress values obtained according to [61].*

** *NYT : Neapolitan Yellow Tuff; NHL : Natural Hydraulic Lime; P : Pozzolanic.*

Comparison between the performances of different types of masonry wallets first shows that unreinforced AM is much more ductile than tuff stone masonry (TSM) and clay brick masonry (CBM). Strengthening masonry with vegetal TRM results in a higher ductility increase, particularly in the case of CBM. Nevertheless, the ductility of strengthened AM is much higher than that of the other two types of strengthened masonry. On the contrary, TRM strengthening is less effective in increasing strength of adobe masonry compared to the other two masonry types. In order to assess the efficiency of H-TRM, performance ratios defined as ratio of strengthened to unreinforced mean values of peak shear stress ($\tau_{max,s}/\tau_{max,u}$) and ductility factor ($\mu_{\gamma,s}/\mu_{\gamma,u}$) are determined and reported in Table 6. Overall, the H-TRM system is characterized by higher strengthening effectiveness when applied to either TSM or CBM with respect to AM, both in terms of strength and ductility. In detail, the strength improvement ($\tau_{max,s}/\tau_{max,u}$) was equal to 2.3 and 5.4, respectively for TSM and CBM, whereas the ductility factor (μ_γ) was 4.6 and 19.8 times that related to unreinforced masonry. As concerns adobe masonry, conversely, a quite limited strength enhancement was obtained ($\tau_{max,s}/\tau_{max,u} = 1.3$), whereas the performance ratio of ductility factor ($\mu_{\gamma,s}/\mu_{\gamma,u}$) equal to 3.6 was in tune with the result obtained for TSM specimens. The reasons for such results could be related to the different matrix used, with low-performance mud mortar applied in the present study opposed to NHL and pozzolanic mortars adopted for matrix in [55]. Furthermore, it is worth notice that experimental results reported in [49] are referred to a TRM system comprising also specific connection devices (hemp ties) potentially able to enhance the strengthening efficiency.

Finally, from the analysis of experimental results reported in [58] and [64], interesting findings can be derived dealing with strengthening performance of TRM systems reinforced with flax grids compared to hemp meshes applied to CBM wallets. The application of a single layer of flax-TRM to CBM wallets produced an average increase in shear strength of approximately 2.2 times, whereas a higher enhancement in ductility was obtained ($\mu_{\gamma,s}/\mu_{\gamma,u} = 4.0$). Therefore, flax-TRM was able to provide similar strengthening performances both in terms of shear strength and ductility compared to H-TRM. Also in this case, the role of the matrix seems not negligible and more experimental data on TRM systems with the same matrix and different reinforcements are needed to achieve comprehensive results.

5 CONCLUSIONS

Within the context of a broad research programme on seismic vulnerability assessment and mitigation of existing adobe buildings, the effectiveness of a strengthening system based on the application of TRM on the external sides of adobe masonry wallets in improving their in-plane shear mechanical performance has been experimentally investigated in this study. Specifically,

diagonal compression tests, suggested by relevant technical codes especially for existing masonry structures (see, e.g., [73–75] amongst others), were carried out on twenty-one AM wallets. Fourteen specimens were strengthened with two TRM solutions, namely, an innovative, non-industrial, hemp-fibre (H) grid and a commercial glass-fibre (G) mesh, whereas identical mud mortar was used.

Mechanical response in terms of shear strains and shear stresses, the latter processed according to both RILEM and ASTM standards, has been provided for all tested specimens that consisted of three series (each including seven wallets), namely URM, H-TRM and G-TRM, discussing the detected damage. Diagonal tension failure mode was observed on unreinforced specimens, with wide passing-through diagonal cracks, partially stair-stepping and involving both joints and bricks due to the similar composition of mud mortar and adobe bricks. Mechanical behaviour was characterized by limited shear strength and rather poor post-peak softening response. Narrowed diagonal cracks developed on adobe wallets strengthened with H-TRM following the stair-stepped direction of the inner unreinforced adobe masonry. The hemp grid gradually reached its ultimate strain up to fracture, and no premature debonding neither local failure was observed.

Measured mechanical responses of wallets belonging to each experimental group was characterized by large dispersion. Therefore, with the aim to extrapolate robust general trends, a statical processing of experimental records was carried out. Specifically, one-way ANOVA was applied to both ductility factor and shear strength values measured for the three independent samples (i.e., URM, H-TRM and G-TRM) and results confirmed the statistical significance of the general trends related to mean values. Accordingly, the H-TRM strengthening system proved to be particularly effective, resulting into a shear strength increase of approximately 25% and an average ductility capacity enhanced by a factor of approximately 3.6. Conversely, G-TRM strengthened specimens showed often local detaching of the TRM system with delamination and debonding phenomena occurred during the post-peak phase. The shear strength of the G-TRM strengthened wallets increased by 12% on average, whereas the mean ductility factor was about twice that related to unreinforced adobe masonry. Therefore, both strengthening solutions were able to improve the in-plane shear capacity of the adobe masonry wallets, particularly in terms of ductility, the latter being a key feature for energy dissipation under earthquake shaking. Experimental results also showed that the H-TRM system is more effective than its G-TRM counterpart because the latter strengthening system is affected by a poor mechanical compatibility between high-performance glass mesh and poor mud mortar. It is further noted that the effectiveness of the strengthening systems was significant even though no transverse connections (e.g., FRP ties) through the thickness of the masonry wallets were installed.

To assess the effectiveness of TRM systems based on vegetable fibres when applied to traditional masonry wallets, a database of experimental shear tests on clay brick or tuff stone masonry wallets available in the literature was properly collected and a comparison of the results was carried out. The application of H-TRM provided considerable improvements in terms of shear strength, with average performance ratios equal to 2.3 and 5.4 for clay brick and tuff stone masonry, respectively. By contrast, ductility capacity was increased of 4.6 times for tuff stone masonry and of approximately 20 times for clay brick masonry. Flax-TRM increased shear strength and ductility of clay brick masonry by factors equal to 2 and 4, respectively, similarly to H-TRM, revealing significant strengthening capacity. It is worth noting that these findings were obtained for different mortar typologies, which definitely play a key role.

In summary, this study shows the possibility to obtain a considerable reduction of seismic vulnerability of existing adobe masonry structures by means of sustainable and cheap TRM system made of mud mortar and hemp fibres, more effective than classical expensive glass fibres. Nevertheless, particular care should be taken regarding manufacturing phase in order to reduce the quite large dispersion of mechanical properties. However, it must be specified that such a beneficial effect on the seismic performance of AM buildings may be obtained provided that local failure modes are properly prevented by improving construction details (e.g., mechanical connections among walls or floors).

Potential developments of this study could focus on the following issues: (i) the influence of mechanical connections to further improve the bond performance of the case-study TRM strengthening system; (ii) the experimental assessment of the TRM strengthening system on full-scale load-bearing walls (with or without openings); and (iii) the shaking table testing and/or numerical seismic response simulation of AM buildings, before and after the application of the TRM strengthening system. This latter part of study would allow evaluating the effectiveness of the TRM strengthening system to prevent local failure modes typically observed on existing AM buildings and to increase the global resistance of the structure.

Acknowledgements

This work was developed under the financial support of the Sardinian Region funding LR N.7 07/08/2007 Year 2011 Tender 3 CRP-48693, that is gratefully acknowledged.

REFERENCES

[1] Houben H, Guillaud H. Earth construction — A comprehensive guide. London: Intermediate Technology Publication; 1994.

[2] Tolles EL, Kimbro EE, Webster FA, Ginell WS. Seismic stabilization of historic adobe structures: Final report of the Getty seismic adobe project. Los Angeles: Getty Publications, 2000.

[3] Briseghella B, Colasanti V, Fenu L, Nuti C, Spacone E, Varum H. Seismic analysis by macroelements of Fujian Hakka Tulous, Chinese circular earth constructions listed in the UNESCO World Heritage List. International Journal of Architectural Heritage 2020; 14(10): 1551-1566.

[4] Correia M. Conservation in Earthen Heritage. Assessment and Significance of Failure, Criteria, Conservation Theory and Strategies. UK: Cambridge Scholars Publishing, 2016.

[5] Blondet M, Garcia GV, Brzev S, Rubiños A. Earthquake-resistant construction of adobe buildings: A tutorial. EERI/IAEE World Housing Encyclopedia, 2003.

[6] Blondet M, Vargas J, Tarque N. Available low-cost technologies to improve the seismic performance of earthen houses in developing countries. In: Proceedings of 14th World Conference on Earthquake Engineering, Bejing, 2008.

[7] Meli R, Hernandez O, Padilla M. Strengthening of adobe houses for seismic actions. In: Proceedings of the Seventh World Conference on Earthquake Engineering, Istanbul, 1980; Vol. 4, p. 465-472.

[8] Caporale A, Parisi F, Asprone D, Luciano R, Prota A. Micromechanical analysis of adobe masonry as two-component composite: Influence of bond and loading schemes. Composite Structures 2014; 112: 254-263.

[9] Sumerente G, Lovon H, Tarque N, Chácara C. Assessment of combined in-plane and out-of-plane fragility functions for adobe masonry buildings in the Peruvian Andes. Frontiers in Built Environment 2020; 6: 52.

[10] Tarque N, Crowley H, Varum H, Pinho R. Displacement-based fragility curves for seismic assessment of adobe buildings in Cusco, Peru. Earthquake Spectra 2012; 28(2): 759-794.

[11] Binici H, Aksogan O, Shah T. Investigation of fibre reinforced mud brick as a building material. Construction and Building Materials 2005; 19(4): 313-318.

[12] Bouhicha M, Aouissi F, Kenai S. Performance of composite soil reinforced with barley straw. Cement and Concrete Composites 2005; 27(5): 617-621.

[13] Achenza M, Fenu L. On earth stabilization with natural polymers for earth masonry construction. Materials and Structures 2006; 39(1): 21-27.

[14] Quagliarini E, Lenci S. The influence of natural stabilizers and natural fibres on the mechanical properties of ancient Roman adobe bricks. Journal of Cultural Heritage 2010; 11(3): 309-314.

[15] Fratini F, Pecchioni E, Rovero L, Tonietti U. The earth in the architecture of the historical centre of Lamezia Terme (Italy): characterization for restoration. Applied Clay Science 2011; 53(3): 509-516.

[16] Vega P, Juan A, Ignacio M, Morán J, Aguado P, Llamas B. Mechanical characterisation of traditional adobes from the north of Spain. Construction and Building Materials 2011; 25: 3020-3023.

[17] Aymerich F, Fenu L, Meloni P. Effect of reinforcing wool fibres on fracture and energy absorption properties of an earthen material. Construction and Building Materials 2012; 27: 66-72.

[18] Adorni E, Coïsson E, Ferretti D. In situ characterization of archaeological adobe bricks. Construction and Building Materials 2013; 40: 1-9.

[19] Wu F, Li G, Li H-N, Jia J-Q. Strength and stress-strain characteristics of traditional adobe block and masonry. Materials and Structures 2013; 46(9): 1449-1457.

[20] Aymerich F, Fenu L, Francesconi L, Meloni P. Fracture behaviour of a fibre reinforced earthen material under static and impact flexural loading. Construction and Building Materials 2016; 109: 109-119.

[21] Aguilar R, Montesinos M, Uceda S. Mechanical characterization of the structural components of Pre-Columbian earthen monuments: Analysis of bricks and mortar from Huaca de la Luna in Perú. Case Studies in Construction Materials 2017; 6: 16-28.

[22] Illampas R, Loizou VG, Ioannou I. Effect of straw fiber reinforcement on the mechanical properties of adobe bricks. In: Proceedings of the 6th Biot conference on poromechanics, Paris, France; 2017.

[23] Rodríguez-Mariscal JD, Solís M, Cifuentes H. Methodological issues for the mechanical characterization of unfired earth bricks. Construction and Building Materials 2018; 175: 804-814.

[24] Li Piani T, Krabbenborg D, Weerheijm J, Koene L, Sluijs LJ. The mechanical performance of traditional adobe masonry components: An experimental-analytical characterization of soil bricks and mud mortar. Journal of Green Building 2018; 13(3): 17-44.

[25] Li Piani T, Weerheijm J, Peroni M, Koene L, Solomos G, Sluys LJ. Dynamic characterization of adobe in compression: the effect of fibre fraction in soil matrix. In: FraMCoS-X: Fracture Mechanics of Concrete and Concrete Structures, Bayonne (France), 2019.

[26] Li Piani T, Weerheijm J, Koene L, Sluys LJ. The Adobe delta damage model: A locally regularized rate-dependent model for the static assessment of soil masonry bricks and mortar. Engineering Fracture Mechanics 2019; 206: 114-130.

[27] Li Piani T, Weerheijm J, Peroni M, Koene L, Krabbenborg D, Solomos G, Sluys LJ. Dynamic behaviour of adobe bricks in compression: The role of fibres and water content at various loading rates. Construction and Building Materials 2020; 230, 117038.

[28] Blondet M, Vargas J, Velasquez J, Tarque N. Experimental study of synthetic mesh reinforcement of historical adobe buildings. In: Proceedings of International Conference on Structural Analysis of Historical Constructions, 2006; p. 715-722.

[29] Turer A, Korkmaz SZ, Korkmaz HH. Performance improvement studies of masonry houses using elastic post-tensioning straps. Earthquake Engineering and Structural Dynamics 2007; 36(5): 683-705.

[30] Dowling DM, Samali B. Low-cost and low-tech reinforcement systems for improved earthquake resistance of mud brick buildings. In: Proceedings of the Getty seismic adobe project 2006 colloquium. Los Angeles, 2006. CA: Getty Conservation Institute.

[31] Charleson A. Seismic strengthening of earthen houses using straps cut from used car tires: a construction guide. Oakland: Earthquake Engineering Research Institute (EERI), 2010.

[32] Blondet M, Vargas-Neumann J, Groenenberg R. Evaluation of the efficacy of mud injection to repair seismic cracks on adobe structures via full-scale shaking table tests. In: Proceedings of 15th World Conference on Earthquake Engineering, Lisboa, 2012.

[33] Torrealva D. Seismic design criteria for adobe buildings reinforced with geogrids. In: Proceedings of 15th World Conference on Earthquake Engineering, Lisboa, 2012.

[34] Bossio S, Blondet M, Rihal S. Seismic behavior and shaking direction influence on adobe wall structures reinforced with geogrid. Earthquake Spectra 2013; 29(1): 59-84.

[35] Blondet M, Vargas J, Sosa C, Soto J. Using mud injection and an external rope mesh to reinforce historical earthen buildings located in seismic areas. In: 9th International

Conference on Structural Analysis of Historical Constructions, Mexico City, 2014. p 14-17.

[36] Sathiparan N, Sakurai K, Numada M, Meguro K. Seismic evaluation of earthquake resistance and retrofitting measures for two story masonry houses. Bulletin of Earthquake Engineering 2014; 12(4): 1805-1826.

[37] Varum H, Parisi F, Tarque N, Silveira D. Structural Characterization and Seismic Retrofitting of Adobe Constructions - Experimental and Numerical Developments, Springer, 2021, https://doi.org/10.1007/978-3-030-74737-4.

[38] Oliveira C, Varum H, Figueiredo A, Silveira D, Costa A. Experimental tests for seismic assessment and strengthening of adobe structures. In: Proceedings of the 14th European conference on earthquake engineering, Ohrid, 2010.

[39] Turanli L, Saritas A. Strengthening the structural behavior of adobe walls through the use of plaster reinforcement mesh. Construction and Building Materials 2011; 25(4): 1747-1752.

[40] Figueiredo A, Varum H, Costa A, Silveira D, Oliveira C. Seismic retrofitting solution of an adobe masonry wall. Materials and Structures 2013; 46(1-2): 203-219.

[41] Miccoli L, Garofano A, Fontana P, Müller U. Experimental testing and finite element modelling of earth block masonry. Engineering Structures 2015; 104: 80-94.

[42] Illampas R, Silva RA, Charmpis DC, Lourenço PB, Ioannou I. Validation of the repair effectiveness of clay-based grout injections by lateral load testing of an adobe model building. Construction and Building Materials 2017; 153: 174-184.

[43] Atzeni C. Stone masonry in rural Sardinian building. Evolution of the traditional building techniques between XIX and XX century. In: Proceedings of the First International Congress on Construction History, Madrid, 2003. p. 279-289.

[44] Parisi F, Asprone D, Fenu L, Prota A. Experimental characterization of Italian composite adobe bricks reinforced with straw fibers. Composite Structures 2015; 122: 300-307.

[45] Ordinanza del Presidente del Consiglio dei Ministri "OPCM 3274", Gazzetta Ufficiale: May 8th, 2003, Ser. Gen 105 (2003) [in Italian].

[46] D.M. 14/01/2008. Norme Tecniche per le Costruzioni (NTC 2008). Gazzetta Ufficiale, Serie Generale n. 29 del 04/02/2008, Supplemento ordinario n.30 [in Italian].

[47] D.M. 17/01/2018. Norme Tecniche per le Costruzioni (NTC 2018). Gazzetta Ufficiale, Serie Generale n. 42 del 20/02/2018, Supplemento ordinario n.8 [in Italian].

[48] Asprone D, Colasanti V, Fenu L, Parisi F, Prota A. Adobe in Sardinia. Static and dynamic behaviour of the earthen material and of adobe constructions. In: Proceedings of the 16th International Brick and Block Masonry Conference, Padova, 2016.

[49] Caporale A, Parisi F, Asprone D, Luciano R, Prota A. Critical surfaces for adobe masonry: micromechanical approach. Composites Part B: Engineering 2014; 56: 790-796.

[50] Caporale A, Parisi F, Asprone D, Luciano R, Prota A. Comparative micromechanical assessment of adobe and clay brick masonry assemblages based on experimental data sets. Composite Structures 2015; 120: 208-220.

[51] Consiglio Superiore dei Lavori Pubblici (CSLP) – Servizio Tecnico Centrale (STC), Linea Guida per la identificazione, la qualificazione ed il controllo di accettazione di compositi fibrorinforzati a matrice inorganica (FRCM) da utilizzarsi per il consolidamento strutturale di costruzioni esistenti (2018) [in Italian].

[52] European Organisation for Technical Assessment (EOTA), EAD 340275-00-0104 "Externally-bonded composite systems with inorganic matrix for strengthening of concrete and masonry structures", 2018.

[53] Bonati A, Franco A, Coppola O, De Luca G. Strengthening of masonry structures: Current national and international approaches for qualification and design. Key Engineering Materials 2019; 817: 501-506.

[54] Turnšek V, Čačovič F. Some experimental results on the strength of brick masonry walls. In: Proceedings of the 2nd International Brick Masonry Conference, Stoke on Trent, 1970. p. 149-156.

[55] EN 1926. Natural stone test methods – determination of compressive strength. Brussels: Comité Européen de Normalisation; 1999.

[56] Yetgin S, Çavdar O, Çavdar A. The effects of the fiber contents on the mechanic properties of the adobes. Construction and Building Materials 2008; 22 (3): 222– 227.

[57] EN 1015-11. Methods of test for mortar for masonry – Part 11: Determination of flexural and compressive strength of hardened mortar. Brussels: Comité Européen de Normalisation; 1999.

[58] Menna C, Asprone D, Durante M, Zinno A, Balsamo A, Prota A. Structural behaviour of masonry panels strengthened with an innovative hemp fibre composite grid. Construction and Building Materials 2015; 100: 111-121.

[59] Mercedes L, Gil L, Bernat-Maso E. Mechanical performance of vegetal fabric reinforced cementitious matrix (FRCM) composites. Construction and Building Materials 2018; 175: 161-173.

[60] ASTM (2015): ASTM E 519-15 – Standard test method for diagonal tension (shear) in masonry assemblages. ASTM International, West Conshohocken, PA, USA.

[61] RILEM TC 76-LUM. Diagonal tensile strength tests of small wall specimens. Bagneux: International Union of Laboratories and Experts in Construction Materials, Systems and Structures; 1994.

[62] Frocht MM. Recent advances in photoelasticity. ASME Transactions 1931; 55: 135-153.

[63] Parisi F, Iovinella I, Balsamo A, Augenti N, Prota A. In-plane behaviour of tuff masonry strengthened with inorganic matrix–grid composites. Composites Part B: Engineering 2013; 45(1): 1657-1666.

[64] Ferrara G, Caggegi C, Martinelli E, Gabor A. Shear capacity of masonry walls externally strengthened using Flax-TRM composite systems: experimental tests and comparative assessment. Construction and Building Materials 2020; 261, 120490.

[65] Parisi F, Balestrieri C, Asprone D. Nonlinear micromechanical model for tuff stone masonry: Experimental validation and performance limit states. Construction and Building Materials 2016; 105: 165-175.

[66] Parisi F, Augenti N. Seismic capacity of irregular unreinforced masonry walls with openings. Earthquake Engineering and Structural Dynamics 2013; 42(1): 101-121.

[67] Losanno D, Ravichandran N, Parisi F, Calabrese A, Serino G. Seismic performance of a low-cost base isolation system for unreinforced brick masonry buildings in developing countries. Soil Dynamics and Earthquake Engineering 2021; 141, 106501.

[68] Portugal H, Tarque N. Non-linear modelling of a geomesh-reinforced earthen wall subjected to dynamic loading. Proceedings of the 11th International Conference on Structural Analysis of Historical Constructions 2018, September 10-13, Cusco, Peru.

[69] Tarque N, Camata G, Spacone E, Varum H, Blondet M. Numerical simulation of an adobe wall under in-plane loading. Earthquakes and Structures 2014; 6(6): 627-646.

[70] Losanno D, Ravichandran N, Parisi F. Comparative assessment of finite element macro-modelling approaches for seismic analysis of non-engineered masonry constructions. Bulletin of Earthquake Engineering, 2021; https://doi.org/10.1007/s10518-021-01180-3.

[71] Mercedes L, Bernat-Maso E, Gil L. In-plane cyclic loading of masonry walls strengthened by vegetal-fabric-reinforced cementitious matrix (FRCM) composites. Engineering Structures 2020; 221, 111097.

[72] ASTM E2126-09, Standard Test Methods for Cyclic (Reversed) Load Test for Shear Resistance of Vertical Elements of the Lateral Force Resisting Systems for Buildings, ASTM International, West Conshohocken, PA, 2009.

[73] EN 1998–3. Eurocode 8: design of structures for earthquake resistance – part 3: assessment and retrofitting of buildings. Brussels: Comité Européen de Normalisation; 2005.

[74] FEMA 356. Prestandard and commentary for the seismic rehabilitation of buildings. Washington (DC): Federal Emergency Management Agency; 2000.

[75] Italian Building Code Commentary. Circolare n. 617 del 02.02.2009: Istruzioni per l'applicazione delle «Nuove Norme Tecniche per le Costruzioni» di cui al decreto ministeriale 14 gennaio 2008. Rome: Italian Ministry of Infrastructures and, Transportation; 2009 [in Italian].